Composition dependence of the band offsets in wurtzite nitridebased heterojunctions

Amel Bhouri, J.-L. Lazzari

Composition dependence of the band offsets in wurtzite nitride-based heterojunctions

Amel Bhouri[1], and Jean-Louis Lazzari[2]

[1] *Laboratoire d'Electronique et Microélectronique, Faculté des Sciences de Monastir, Université de Monastir, Tunisie.*

[2] *Aix-Marseille Université, CNRS, CINaM UMR CNRS 7325, Case 913, Campus de Luminy, 13288 Marseille cedex 9, France.*

ABSTRACT

We theoretically calculate the composition dependence of the valence- and conduction- band discontinuities at the interfaces between selected III-nitride ternary materials with wurtzite structure, e.g. $Al_xGa_{1-x}N/Al_xGa_{1-x}N$, $In_xGa_{1-x}N/In_xGa_{1-x}N$ and $In_xA_{1-x}N/In_xA_{1-x}N$. Calculations are performed using a theoretical model, initially proposed by S. L. Chuang et al. **[1]**. Depending on a particular set of input parameters, simulation results show that band offsets change more or less with strain. The valence band offsets, together with the resulting conduction band offsets, indicate that a type -I, type- II band line-up forms at $In_xGa_{1-x}N/GaN$, $Al_xGa_{1-x}N/GaN$ heterojunctions with varying In, Al contents respectively. Also, based upon the same model, we propose a type I Indium- dependent band alignment in $In_xAl_{1-x}N/AlN$ interfaces. The failure of the transitivity rule, which is often used to determine the band offsets in heterojunctions, was demonstrated and its cause was explained. The obtained results are well compared with experiment and theory in various reliable test cases and therefore provide a basis for optimization and design of novel interface structures.

Keywords: Wurtzite nitrides, Heterojunctions, Strain, Band offsets.

Corresponding author: bhouri_amel@yahoo.fr

Tel: +216 52 67 60 42

1-INTRODUCTION

The group III-nitrides and their alloy systems are emerging as the important class of semiconductor compounds for optoelectronic and electronic applications. Since the demonstration of high-efficiency InGaN blue LEDs by Nakamura et al. **[2]**, nitrides have found their way into many commercial optoelectronics device applications. Large progress on the growth of devices based on such materials was achieved and a great interest is given to the realization of quantum devices using GaN-based material. Indeed, AlN, GaN, InN and their alloys AlGaN, InGaN and InAlN, have attracted immense attention owing to their outstanding properties such as wide band-gap energy, high peak electron velocity, high saturation electron velocity, and high thermal stability **[3,4]**.

The band gap energy of InGaN, ranging from the near infrared (0.7 eV) to the ultraviolet (3.4 eV), makes such alloy a promising candidate for radiation-resistant multi-junction solar cells **[5, 6]**. $In_xAl_{1-x}N$ is attracting more and more attention for its interesting characteristics, in particular, (i) it covers a large bandgap energy range spanning from the deep infrared to the far ultraviolet and (ii) it can be in-plane lattice matched to GaN with In composition around $x = 0.18$. Thus, $In_xAl_{1-x}N$ is holding much potential for use in a variety of optoelectronic and electronic device applications such as distributed Bragg reflectors and high-electron mobility transistors. Furthermore, III-nitride semiconductors are characterized by a large conduction band discontinuity (1.75 eV between GaN and AlN **[7]**), which makes GaN/AlGaN heterostructures of great interest for intersubband optoelectronics both in the near infrared and in the terahertz spectral ranges. Thanks to the high energy of their longitudinal optical phonon modes (92 meV in GaN), III-nitrides are excellent candidates for the fabrication of high temperature THz quantum cascade lasers QCLs **[6]**.

Under ambient conditions, the thermodynamically stable structure for bulk AlN, GaN, InN and their ternaries along with the quaternary is wurtzite (wz). Furthermore, wz group-III nitrides are piezoelectric, in which large spontaneous polarizations exist along the c axis (polar axis). Moreover, depending on the degree of lattice mismatch, the piezoelectric effect also contributes to the polarization fields to a certain extent. The discontinuity of polarization across a heterojunction manifests itself as fixed interface bound polarization charges and induces the “built-in electric field”, which is a vital parameter in determining bandgaps, band structure and other electronic properties **[8, 9]**. For transport modelling, of a whole multilayered device stack, such “built-in electric field” is generally treated within Schrödinger-Poisson-transmittance models **[10]**.

To manipulate the electrical, optical, and transport properties in nitride based devices effectively, an accurate determination of the basic properties of wurtzite nitride based heterostructures is crucial. The valence band offset (VBOs) and conduction band offsets (CBOs) between two alloys are the key parameters to the design heterostructures- based, $Al_xGa_{1-x}N$, $In_xGa_{1-x}N$ and $In_xAl_{1-x}N$ optoelectronic devices. In fact, a precise knowledge of the latter quantities is vital for evaluating the degree of the localization of charges at the interfaces of semiconductor multilayers, the degree of carrier confinement and therefore the usefulness of the material for device applications.

Experimental **[11-14]** and theoretical **[1, 15-28]** methods have been a serious challenge in determining valence and conduction band offsets of semiconductor heterojunctions. The authors of reference **[1]** have proposed a theoretical model for calculating the band structure of strained quantum well wurtzite semiconductors including strain effects on the shifts of band edges. They have applied their model for the calculation of GaN/AlGaN band offset heterojunction. Information about band offsets at further homovalent and heterovalent **[29, 30]** wurtzite nitride heterojunctions is still lacking. This has inspired us to perform and update band offset calculations, using the model detailed in reference **[1]**, at variety of wurtzite nitride based interfaces with taking advantage of the outcomes of recent improvements in epitaxial growth of III-nitrides.

The organization of the present paper is as follows. In section 2, we describe the intended theoretical model and we give the computational details of the band offset calculations. In section 3, we calculate the band offsets and the strained band gaps of the considered heterojunctions $Al_xGa_{1-x}N/Al_yGa_{1-y}N$, $In_xGa_{1-x}N/In_yGa_{1-y}N$ and $In_xA_{1-x}N/In_yA_{1-y}N$ and their dependence on aluminum and indium compositions respectively. In section 4, we focus on the discussion of the obtained results. Finally, section 5 summarizes the present work.

2-THEORITICAL BACKGROUND

2-1 Band edge energies:

We consider a wurtzite strained interface (material-1/material-2), pseudomorphically grown along the (0001) (c-axis) direction. We note that practical growth of such structure is only possible for layers that do not exceed a certain critical thickness which depends on the material and on the degree of lattice mismatch **[23]**. To predict the band lineup at strained interfaces, the first step is to obtain values of the band lineups at ideal interfaces and after one

must include the appropriate strain in each of the materials to construct a pseudomorphic interface **[23]**.

In contrast to zinc blend materials, the wurtzite structure does not give a triply degenerate valence band edge **[31]**. For the unstrained system, the HH and LH bands are doubly degenerate and the CH band is split off by the crystal field splitting Δ_1 which is in general not related to the spin orbit interaction **[31]**. In principle, two different spin orbit splitting parameters exist ($\Delta_2$and Δ_3); they are commonly assumed equal and are allied to the spin orbit splitting Δ_{so} by the following relation:

$$\Delta_2 = \Delta_3 = \frac{\Delta_{so}}{3} \tag{1}$$

Consequently, adding the spin orbit interaction to the crystal field effect, the valence band-edge energies for strain free wurtzite semiconductor layers are given, with respect to reference energy E_v^0 by: **[1]**

$$E_{iv,1}^{uns} = E_v^0 + \Delta_1 + \Delta_2 \tag{2-a}$$

$$E_{iv,2}^{uns} = E_v^0 + \frac{\Delta_1 - \Delta_2}{2} + \sqrt{\left(\frac{\Delta_1 - \Delta_2}{2}\right)^2 + 2\Delta_3^2} \tag{2-b}$$

$$E_{iv,3}^{uns} = E_v^0 + \frac{\Delta_1 - \Delta_2}{2} - \sqrt{\left(\frac{\Delta_1 - \Delta_2}{2}\right)^2 + 2\Delta_3^2} \tag{2-c}$$

where i denotes the semiconductor material (1 or 2) and the subscripts 1, 2 and 3 in $E_{iv,1}^{uns}$, $E_{iv,2}^{uns}$ and $E_{iv,3}^{uns}$ stand for heavy hole (HH), light hole (LH) and crystal field split off (CH) respectively.

The lattice constant mismatch between the material (1 or 2) and the substrate gives rise to a strain in the layer described by the following equations:

$$\varepsilon_{xx} = \varepsilon_{yy} = \frac{a_0 - a}{a} \tag{3-a}$$

$$\varepsilon_{zz} = -\frac{2C_{13}}{C_{33}}\varepsilon_{xx} \tag{3-b}$$

where a_0 and a are the lattice constants of the substrate and the strained material respectively. C_{ij} designate the elastic constants.

We note that for wurtzite structures, the valence-band-mixing between the three valence bands (heavy hole (HH), light hole (LH) and crystal field split off (CH)), strongly coupled, and has to be taken into account with the aim to take full advantage of the strained structure and to obtain better designs **[1]**. In fact, the strain affects the valence band edges and so influences the band discontinuity at the strained layer interfaces. According to reference **[1]**, under strain, the valence band edge-energies are given by:

$$E_{iv,1}^{str} = E_v^0 + \Delta_1 + \Delta_2 + \theta_\epsilon + \lambda_\epsilon \tag{4-a}$$

$$E_{iv,2}^{str} = E_v^0 + \frac{\Delta_1 - \Delta_2 + \theta_\epsilon}{2} + \lambda_\epsilon + \sqrt{\left(\frac{\Delta_1 - \Delta_2 + \theta_\epsilon}{2}\right)^2 + 2\Delta_3^2} \quad (4\text{-b})$$

$$E_{iv,3}^{str} = E_v^0 + \frac{\Delta_1 - \Delta_2 + \theta_\epsilon}{2} + \lambda_\epsilon - \sqrt{\left(\frac{\Delta_1 - \Delta_2 + \theta_\epsilon}{2}\right)^2 + 2\Delta_3^2} \quad (4\text{-c})$$

$$\lambda_\epsilon = D_1\varepsilon_{zz} + D_2(\varepsilon_{xx} + \varepsilon_{yy}) \quad (5)$$

$$\theta_\varepsilon = D_3\varepsilon_{zz} + D_4(\varepsilon_{xx} + \varepsilon_{yy}) \quad (6)$$

we note that λ_ϵ and $\theta_\varepsilon$depend on the deformation potentials $D_{1,2,3,4}$.

The procedure outlined above for valence bands also applies for conduction bands. In strained free semiconductor system, the conduction band edge E_{ic}^0 is above the top valence band with band gap energy E_g. Adding strain effects, the conduction band edge has an hydrostatic energy shift $P_{c\varepsilon}$:

$$E_{ic} = E_{ic}^0 + P_{c\varepsilon} \quad (7)$$

$$P_{c\varepsilon} = a_{cz}\varepsilon_{zz} + a_{ct}(\varepsilon_{xx} + \varepsilon_{yy}) \quad (8)$$

We note that a_{cz} and a_{ct} are the conduction band deformation potentials which are usually assumed to be equal for simplicity **[1]** and are generally combined with the valence band deformation potentials D_1 and D_2 respectively **[32]**.

2-2 Band offsets

The valence $(\Delta E_{v,1,2,3}^{str})$ and conduction (ΔE_c^{str}) band discontinuities of an heterojunction (material-1/material-2) may then be estimated by the difference between the individual band-edge energies of the strained materials (material 1and material 2) and are described by the following equations:

$$\Delta E_{v,1,2,3}^{str} = E_{v,1,2,3}^{str}(material_1) - E_{v,1,2,3}^{str}(material_2) \quad (9)$$

$$\Delta E_c^{str} = E_c^{str}(material_1) - E_c^{str}(material_2) \quad (10)$$

We point out that, in the case where material 2 is strain free, the last equations will satisfy:

$$\Delta E_{v,1,2,3}^{str} = E_{v,1,2,3}^{str}(material_1) - E_{v,1,2,3}^{uns}(material_2) \quad (11)$$

$$\Delta E_c^{str} = E_c^{str}(material_1) - E_c^{uns}(material_2) \quad (12)$$

here, the subscript uns labels the strain free valence band edges (see equation 2).

3-SIMULATION RESULTS

3-1 Bulk properties

Firstly, we consider the basic properties of the parent compounds-wz bulk AlN, GaN and InN. The lattice constants, energy parameters, deformation potentials and elastic constants are taken mostly from recent references and are listed in table-1 **[31-33]**. For the

derived ternary compounds, the linear interpolation formula between the pure materials is appropriate for most of the material parameters except for energy band gaps. The analytical expression of a bulk $A_xB_{1-x}N$ band gap is defined through:

$$E_g(A_xB_{1-x}N) = xE_g(AN) + (1-x)E_g(BN) - bx(1-x) \quad (13)$$

where b is the bowing parameter measuring the deviation from linear dependence of the band gap on x and $E_g(AN, BN)$ is the energy band gap of the binary materials. Values of 0.62, 1.36 and 2.5 eV have been reported for the bowing parameters of relaxed- $Al_xGa_{1-x}N$, $In_xGa_{1-x}N$ and $In_xAl_{1-x}N$ respectively **[34-36]**.

Table 1: AlN, GaN and InN physical parameters.

Parameter	AlN	GaN	InN
Lattice constant (Å)			
a	3.112	3.189	3.54
c	4.982	5.185	5.703
Energy parameters			
E_g (eV)	6.25	3.51	0.69
$\Delta_1=\Delta_{cr}$ (meV)	-0.164	0.019	0.041
$\Delta_{so}=3\Delta_2=3\Delta_3$ (meV)	0.019	0.014	0.001
Valence band edge energy (eV)	-3.44	-2.64	-1.59
Deformation potentials (eV)			
ac	-6.4	-5.4	-1.7
a_{cz}-D_1	-4.31	-5.81	-3.62
a_{ct}-D_2	-12.11	-8.92	-4.60
D_3	9.12	5.47	2.68
D_4	-3.79	-2.98	-1.74
Elastic constants (GPa)			
C_{13}	108	106	92
C_{33}	373	398	224

As we have mentioned above (equation 2), the valence band edges for given semiconductor materials are measured from a reference energy E_v^0 **[1]**. Therefore, to perform band offset calculation, one has to found the reference band-edge energies E_v^0 for all binary and ternary nitrides considered in these calculations. Because of the different sign of the crystal field splitting energy (Δ_1) of the three binary compounds, GaN, AlN and InN, there are different arrangements of the energy levels. Since the GaN and InN crystal field splittings (Δ_1) are positives, $E_{v,1}^{uns}$ (E_{HH}) is then the highest level in both GaN and InN. However $E_{v,2}^{uns}$ (E_{LH}) plays analogous role in AlN which has a negative crystal field splitting. We approximate the

location of E_v^0 in each ternary alloy ($Al_xGa_{1-x}N$, $In_xGa_{1-x}N$ and $In_xAl_{1-x}N$) with a linear interpolation of its related binaries.

3-2 Strained $A_xB_{1-x}N/A_yB_{1-y}N$ systems

The lattice-mismatch between the materials $A_xB_{1-x}N$ and $A_yB_{1-y}N$ introduces tensile or compressive strains as being described by equations 3. Such a strain shifts individually the valence band edges $E_{iv,1}^{str}$ (HH), $E_{iv,2}^{str}$(LH) and $E_{iv,3}^{str}$(CH) (see equation 4). Therefore, for heterojunction problem, it is essential to calculate values for individual band edges, since they influence the discontinuities at the interface. For the investigation of $A_xB_{1-x}N/A_yB_{1-y}N$ valence band offsets, we have started by calculating the energy difference between the individual valence band edges (HH, LH, CH) of the strained-$A_xB_{1-x}N$ layer and the upper valence energy level of the relaxed- $A_yB_{1-y}N$ material. In a second step, we have determined the energy band discontinuities between the top energy level of strained-$A_xB_{1-x}N$ and the upper energy level in the relaxed- $A_yB_{1-y}N$ layers.

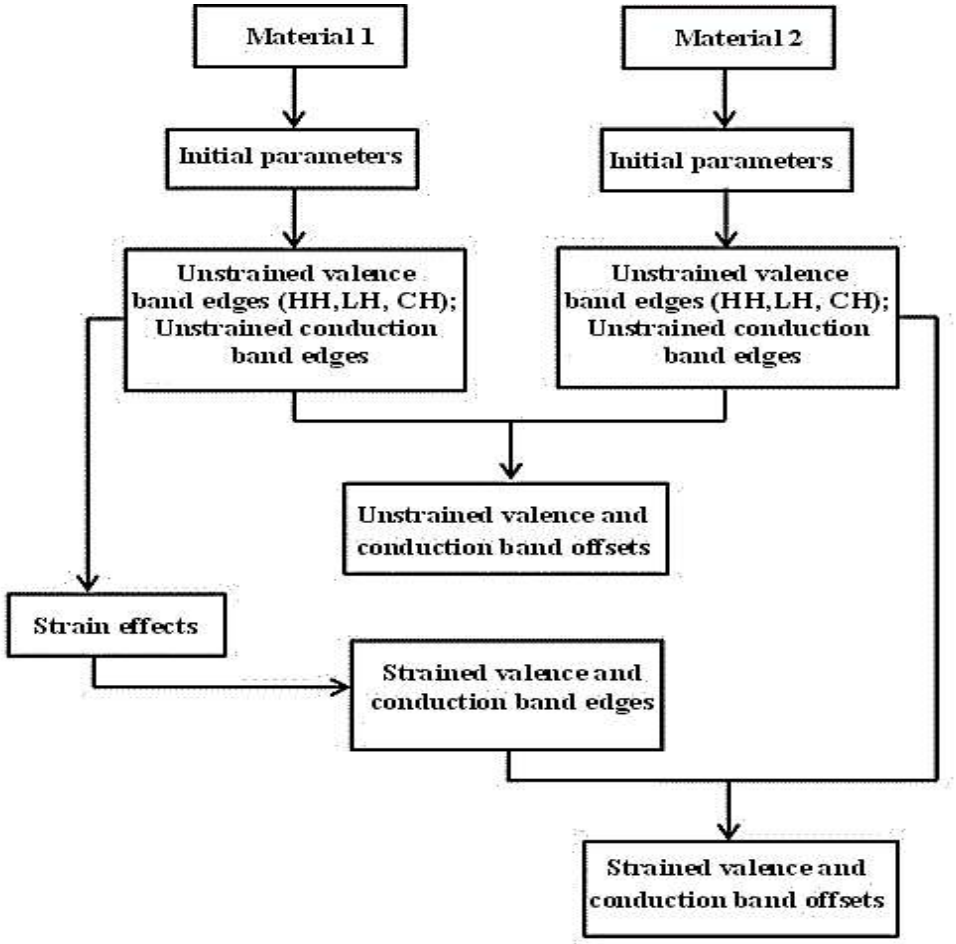

Figure 1: Flowchart indicating the major steps of band offset calculations.

Equations 14 and 15 describe the outlined process:

$$\Delta E_{v,1,2,3}^{str}\left(A_xB_{1-x}N\ /A_yB_{1-y}N\right) = E_{v,1,2,3}^{str}(A_xB_{1-x}N) - E_v^{uns}(A_yB_{1-y}N) \quad (14)$$

$$\Delta E_{v}^{str}\left(A_xB_{1-x}N\ /A_yB_{1-y}N\right) = E_{v}^{str}(A_xB_{1-x}N) - E_v^{uns}(A_yB_{1-y}N) \quad (15)$$

we note that E_v^{uns} and E_v^{str} stand for the top valence band energy of the relaxed and strained material correspondingly.

Similar equations are applied to obtain conduction band offsets for strained heterojunctions:

$$\Delta E_{c}^{str}\left(A_xB_{1-x}N\ /A_yB_{1-y}N\right) = E_{c}^{str}(A_xB_{1-x}N) - E_c^{uns}(A_yB_{1-y}N) \quad (16)$$

Where, E_c^{uns} (E_c^{str}) is the lowest conduction band edge of the unstrained (strained) material. The overall process calculating the band discontinuities between two materials is described in a form of a general flowchart illustrated in figure 1.

3-2-1 Strained $Al_xGa_{1-x}N/Al_yGa_{1-y}N$ system

Using the above set of equations together with the list of parameter values cited in table1, we have calculated the valence- ($\Delta E_{v,1,2,3}^{str}$, ΔE_v^{str}) and conduction- (ΔE_c^{str}) band discontinuities in the (0001) (c-axis) direction between strained- $Al_xGa_{1-x}N$ on relaxed $Al_yGa_{1-y}N$ layers in the whole range of compositions. Figure 2(a) summarizes the obtained results for strained VBOs: $\Delta E_{v,1}^{str}$, $\Delta E_{v,2}^{str}$ and $\Delta E_{v,3}^{str}$. Figure 2(b) illustrates only the VBOs corresponding to energy difference between the top valence bands of the two considered interface materials with and without taking into account the strain effects. Figure 3 simply displays the strained and unstrained conduction band offsets between the lowest conduction bands and the strain contour plots calculated on the basis of equation (3-a).

The performed numerical simulations highlight the amount of strain in the alloy layers and illustrate the strong dependence of the band offsets on compositions. In fact, $Al_xGa_{1-x}N$ alloy is tensile strained on $Al_yGa_{1-y}N$ relaxed material in the case $x > y$ and compressively strained in the case $x < y$. Figure 2(a) shows the dissimilar demeanors of $\Delta E_{v,1}^{str}$, $\Delta E_{v,2}^{str}$ and $\Delta E_{v,3}^{str}$ as a function of composition. Such behaviors arise from the deformation potential corrections and the local induced strain.

As displayed in figure 2(b), the rate change of the valence band offset is different from tensile to compressive strain. When we include the tensile strain effects ($x > y$), we note a strong variation of the VBOs compared with the situation when only the spin orbit interaction is included to the crystal field effect.

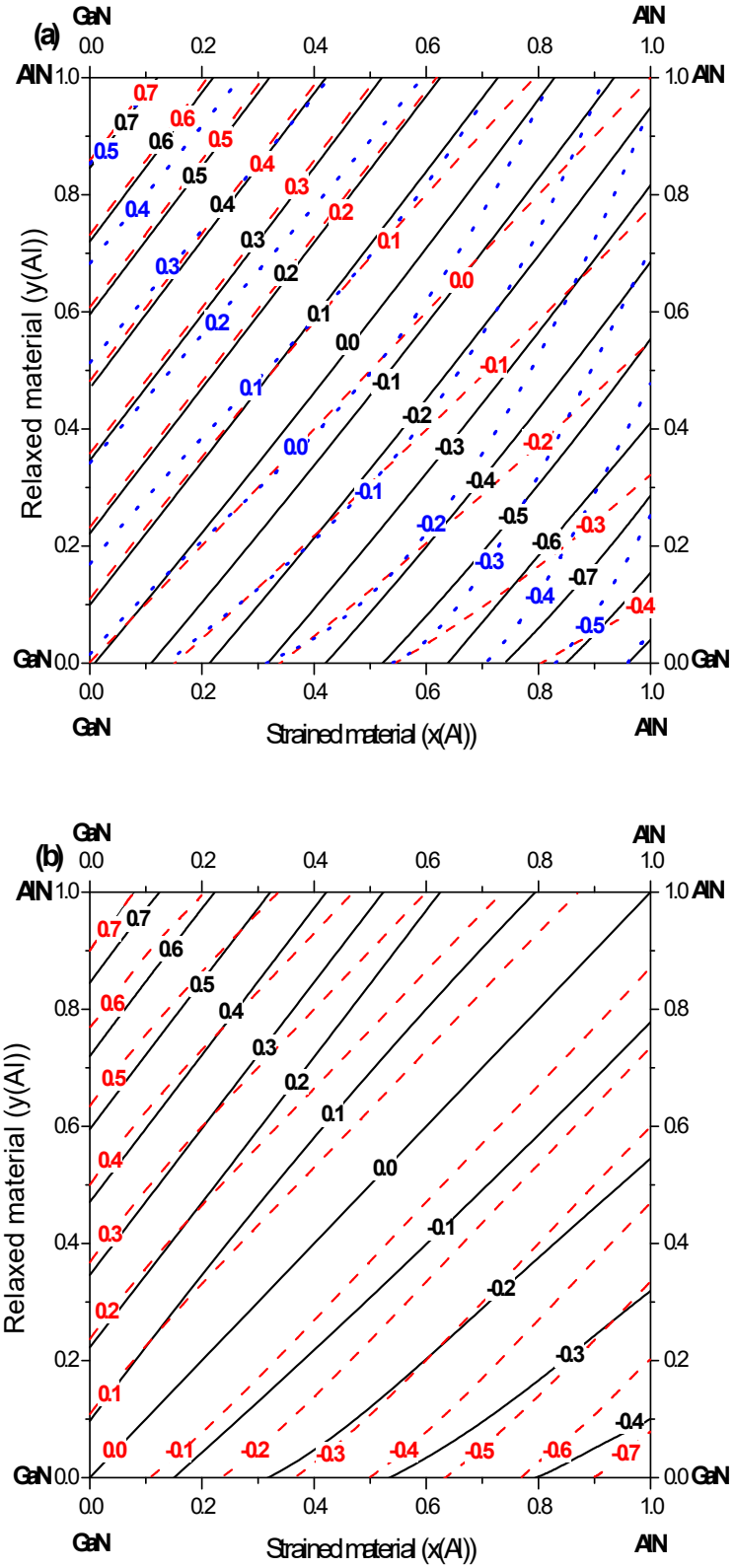

Figure 2: The contour plots of $Al_xGa_{1-x}N/Al_yGa_{1-y}N$ valence band offsets, (a): $\Delta E_{v,1}^{str}$ (black solid lines), $\Delta E_{v,2}^{str}$ (red dashed lines) and $\Delta E_{v,3}^{str}$ (blue dotted lines); (b): ΔE_v^{uns} (dashed lines), ΔE_v^{str} (solid lines) as a function of compositions x and y.

For the unstrained AlN/GaN heterostructure, $\Delta E_v^{uns} \approx -0.8\ eV$ is derived and for the strained AlN/GaN interface the VBO (ΔE_v^{str}) turn into a reduced value of about $-0.46\ eV$. However, under compressive strain ($x < y$) the GaN/AlN VBO is not very affected by strain ($\Delta E_v^{uns} \approx 0.8\ eV$ and $\Delta E_v^{str} = 0.825\ eV$). The differences between the values for the strained and ideal interfaces are in the order of $0.34\ eV$ and $0.025\ eV$ for AlN/GaN and GaN/AlN interfaces respectively.

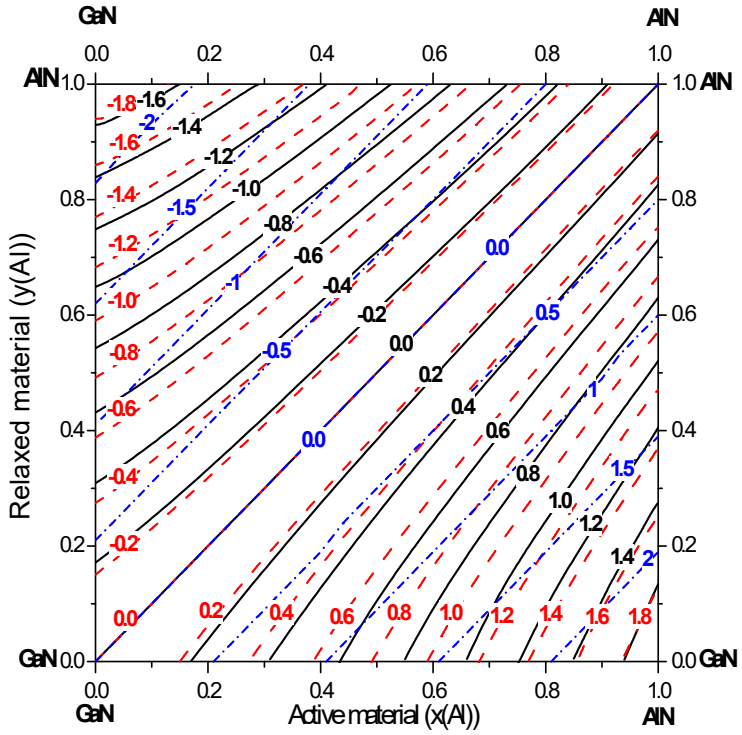

Figure 3: Strained (solid lines) and unstrained (dashed lines) conduction band offsets at $Al_xGa_{1-x}N/Al_yGa_{1-y}N$ heterointerfaces. In blue color are displayed the contour plots of lattice-mismatch induced strain (%).

From figure 3, it is clear that the conduction band offsets ΔE_c^{str} are less affected by strain compared to the valence band offsets but reach very large values with a maximum of about $-1.8\ eV$ and $1.75\ eV$ in GaN/AlN and AlN/GaN strained heterojunction respectively. The unstrained CBO value for GaN/AlN (AlN/GaN) is calculated to be equal to about $-2.0\ eV$ ($2.0\ eV$).

As can be deduced from the valence and conduction band offsets (plots 2 and 3), the lineups at $Al_xGa_{1-x}N/GaN$ $(x > y)$ and $GaN/Al_yGa_{1-y}N$ $(x < y)$ strained/relaxed heterojunctions are found to be of "type I" in the GaN layer. Hence, for both interfaces, the carriers are confined in the GaN region. The obtained results are approximately fitted by the followings analytical expression model:

$$\Delta E_{v,c} = (x - y)\{(ax + b) + (cx + d)(x + y)\} \qquad (17)$$

The parameters $a, b, c\ and\ d$ are given in eV and are cited in table 2. In the same table also are given the errors on the calculated ΔE_v^{str} and ΔE_c^{str}.

3-2-2 Strained $In_xGa_{1-x}N/In_yGa_{1-y}N$ system

We apply the same approach detailed above to calculate the band offsets at $In_xGa_{1-x}N/In_yGa_{1-y}N$ heterojunction. The $In_xGa_{1-x}N/In_yGa_{1-y}N$ band offsets and strain contour plots are displayed in figures 4 and 5 as a function of x and y. We show the $\Delta E_{v,1,2,3}^{str}$ valence band discontinuities in figure 4(a) and the ΔE_v^{str} (ΔE_v^{uns}) in figure 4(b). It is important to mention that, the $In_xGa_{1-x}N$ material is under compressive strain when $x > y$ and under tensile strain elsewhere. It is well established that the band gap of $In_xGa_{1-x}N$ is sensitive to composition, thus its band offsets would also be influenced by composition and strain. Overall, the calculated $In_xGa_{1-x}N/In_yGa_{1-y}N$ band offsets show the following trends:

(i) Figure 4(a) clearly illustrate that the valence band discontinuities $\Delta E_{v,1}^{str}$ and $\Delta E_{v,3}^{str}$ show nearly linear variation versus x and y when subject to both compressive and tensile strain. The tensile strain in $In_xGa_{1-x}N$ leads to a positive bowing of the variation of $\Delta E_{v,2}^{str}$ as a function of compositions x and y. Nonetheless, under compressive strain, $\Delta E_{v,2}^{str}$ presents linear variation versus compositions.

(ii) In the case of compressive strain ($x > y$), the valence and conduction band offsets of $In_xGa_{1-x}N/In_yGa_{1-y}N$ heterojunction do not change much with strain compared to the case when no strain effects are included. Under 10% of compressive strain, the InN/GaN valence and the conduction band offsets are shifted only of about $0.15\ eV$ and $0.2\ eV$ respectively and we assume $\Delta E_v^{str} = 1.2\ eV$ ($\Delta E_v^{uns} = 1.05\ eV$) and $\Delta E_c^{str} = -1.57\ eV$ ($\Delta E_c^{uns} = -1.77\ eV$) .

(iii) Compared to the unstrained situation, the tensile strain ($x < y$) strongly shifts the VBO and CBO to lower energies. For just over 10% tensile strain, we calculate the values $\Delta E_v^{str} = -0.323\ eV$ ($\Delta E_v^{uns} = -1.05\ eV$) and $\Delta E_c^{str} = 0.9\ eV$ ($\Delta E_c^{uns} = 1.77\ eV$) for GaN/InN heterointerface.

(iv) As it is shown in figures 4(b) and 5, when $x > y$ the valence offsets present positive values and the conduction offsets present negative values, however the opposite trend is observed when $x < y$. Consequently, a type I lineup forms separately, in $In_xGa_{1-x}N$ strained layer when subject to compressive strain and, in $In_yGa_{1-y}N$ relaxed layer when subject to tensile strain.

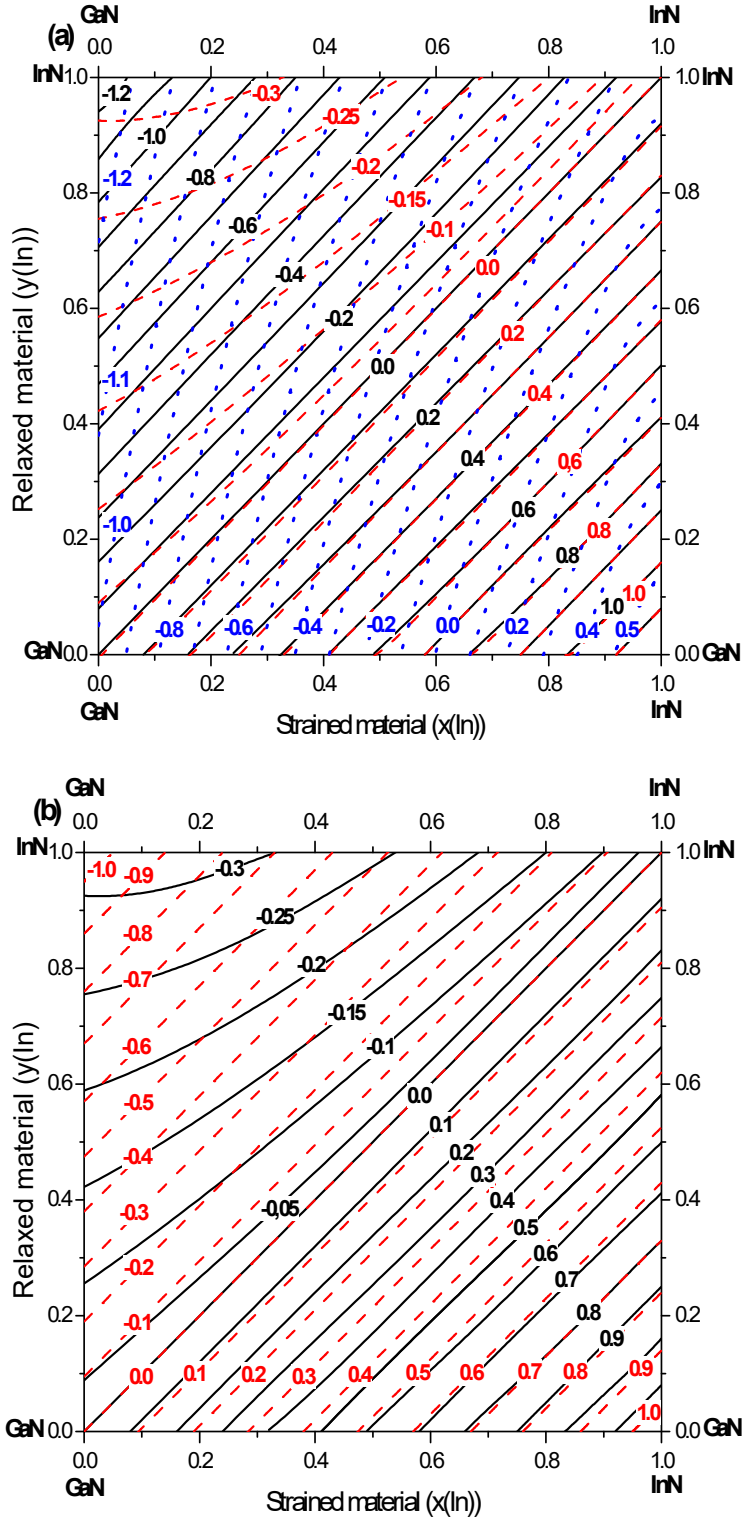

Figure 4: The contour plots of $In_xGa_{1-x}N/In_yGa_{1-y}N$ valence band offsets, (a): $\Delta E_{v,1}^{str}$ (black solid lines), $\Delta E_{v,2}^{str}$ (red dashed lines) and $\Delta E_{v,3}^{str}$ (blue dotted lines); (b): ΔE_v^{uns} (dashed lines), ΔE_v^{str} (solid lines) as a function of compositions x and y.

The band offsets of $In_xGa_{1-x}N/In_yGa_{1-y}N$ heterojunction are approximately fitted according to equation 17. Values of parameters a, b, c and d are cited in table 2.

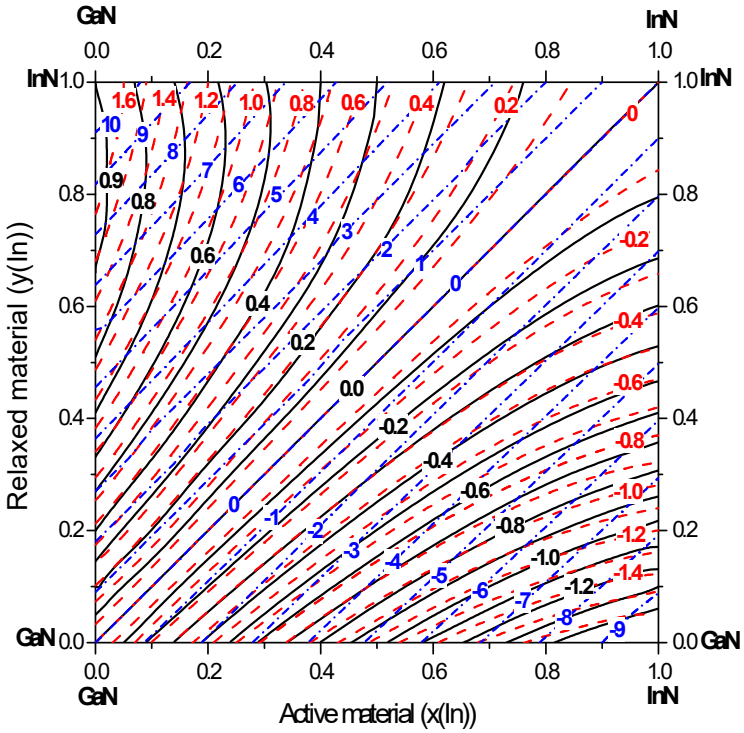

Figure 5: Strained (solid lines) and unstrained (dashed lines) conduction band offsets at $In_xGa_{1-x}N/In_yGa_{1-y}N$ heterointerfaces. In blue color are displayed the strain contour plots (%).

3-2-3 Strained $In_xAl_{1-x}N/In_yAl_{1-y}N$ system

Following the previously approach (equations 13-14) used in evaluating band discontinuities at strained $Al_xGa_{1-x}N/Al_yGa_{1-y}N$ and $In_xGa_{1-x}N/In_yGa_{1-y}N$ interfaces, we have calculated the VBO and CBO of $In_xAl_{1-x}N/In_yAl_{1-y}N$ heterojunction in the entire indium range. The obtained results are summarized in figures 6 and 7 where are exhibited the energy contour plots of strain and band offsets $\Delta E_{v,1,2,3}^{str}$, ΔE_v^{str} and ΔE_c^{str} as a function of indium compositions. When Indium composition is changed, strain is variably introduced in $In_xAl_{1-x}N$. Thus, the resulting strained layer is compressively strained for $x > y$ or tensile strained in the case $x < y$. The curves displayed in figure 6 and 7 demonstrate the following key features:

(i) $\Delta E_{v,2}^{str}$ (LH) and $\Delta E_{v,3}^{str}$ (CH) exhibit nonlinear variation in the domain compositions $x < y$ and $x > y$ respectively. In addition, composition dependence of $\Delta E_{v,2}^{str}$ shows a concave behavior indicating the presence or a large bowing parameter. Yet, the evolution of $\Delta E_{v,1}^{str}$ as a function of x and y remains linear whether in the tensile or in the compressive region.

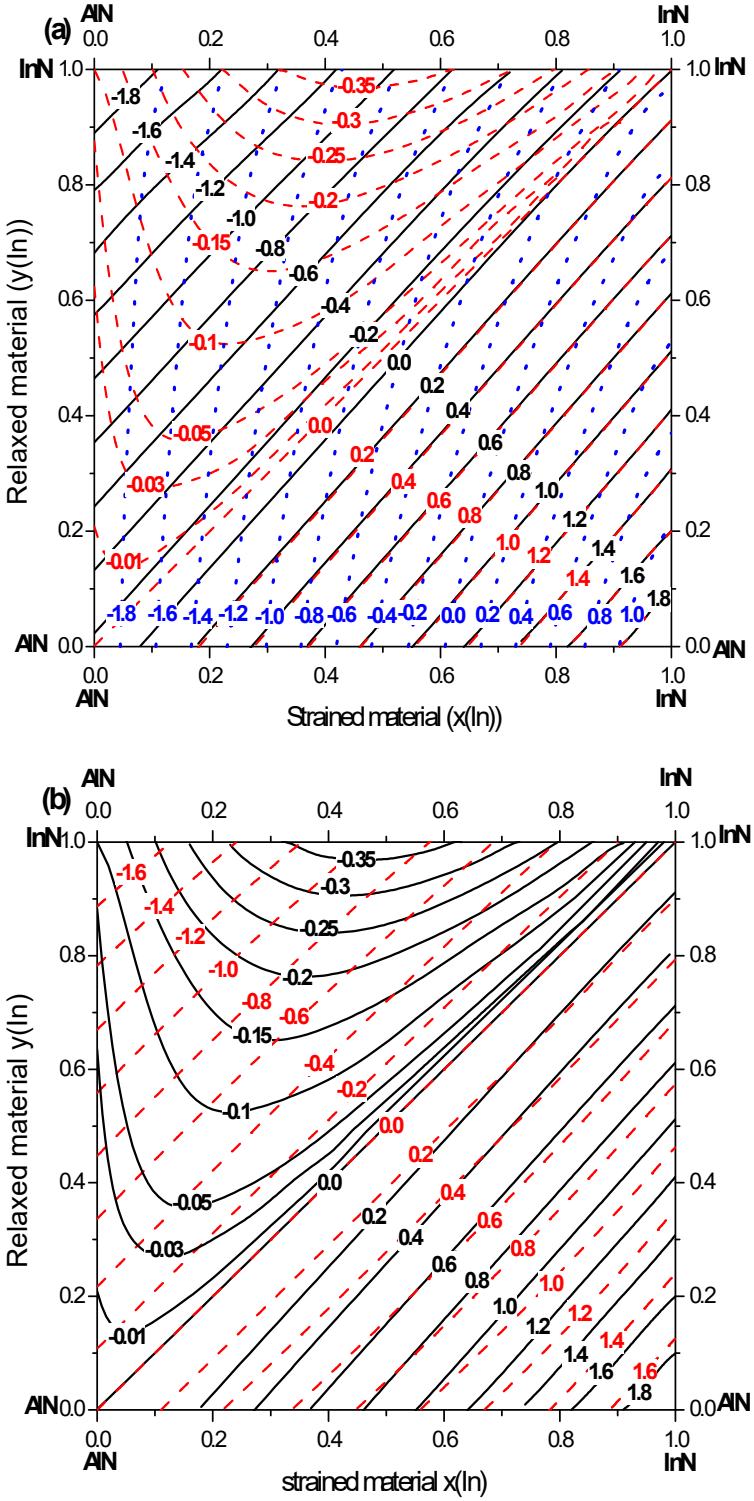

Figure 6: The contour plots of $In_xAl_{1-x}N/In_yAl_{1-y}N$ valence band offsets, (a): $\Delta E_{v,1}^{str}$ (black solid lines), $\Delta E_{v,2}^{str}$ (red dashed lines) and $\Delta E_{v,3}^{str}$ (blue dotted lines); (b): ΔE_v^{uns} (dashed lines), ΔE_v^{str} (solid lines) as a function of compositions x and y.

(ii) From figure 6(b), one can realize that under tensile strain ($x < y$), the VBOs ΔE_v^{str} are considerably influenced by strain and present a nonlinear behavior in comparison with their variation at free strain (ΔE_v^{uns}). When InN is used as relaxed material, the $In_xAl_{1-x}N$/InN valence band offsets increase and then decrease with x. We obtain a value around $-0.09\ eV$ under strain instead of $-1.85\ eV$ at zero strain. In the case when $x > y$, VBOs change a little with strain and we obtained values of about $2.0\ eV$ and $1.85\ eV$ for the VBOs of strained and unstrained InN/AlN respectively.

(iii) The CBO ΔE_c^{str} is also highly influenced by tensile strain than by compressive strain. Even though the CBO bowing is somewhat small for the entire range of In composition, we clearly notice that the AlN/InN CBO is significantly red-shifted by approximately $0.95\ eV$ under about 14% tensile strain. In fact we obtained values of $2.48\ eV$ and $3.77\ eV$ for the AlN/InN conduction band discontinuities with and without taking into account the strain respectively. However, for the InN/AlN interface, the CBO is slightly reduced under strain and we calculate the values $-3.5\ eV$ and $-3.77\ eV$ for strained and unstrained heterointerface respectively.

(iv) From figure 6 and 7, we identify two type lineups depending on the amount of Indium in the strained-$In_xAl_{1-x}N$ layer. As it can be noted, a type I heterojunction is seen to be formed separately in $In_xAl_{1-x}N$ when $x > y$, and in $In_yAl_{1-y}N$ elsewhere.

Table 2: Fitted parameters of equation 17 describing the variation of valence and conduction band offsets at the different studied nitride interfaces. Values of a, b, c and ε are in eV.

	$Al_xGa_{1-x}N/Al_yGa_{1-y}N$		**$In_xAl_{1-x}N/In_yAl_{1-y}N$**		**$In_xGa_{1-x}N/In_yGa_{1-y}N$**	
	ΔE_c	ΔE_v	ΔE_c	ΔE_v	ΔE_c	ΔE_v
a	0.0034	0.5073	-1.201	2.847	-0.7407	1.23
b	1.116	-0.8162	-3.883	0.4535	-2.243	0.6877
c	-0.0371	-0.0614	0.1917	-0.2913	0.0658	-0.0877
d	0.6729	-0.0228	1.345	-0.5112	1.328	-0.5048
ε	$5x10^{-4}$	$2.5x10^{-3}$	$5x10^{-5}$	$3.17x10^{-2}$	$1.88x10^{-5}$	$2.38\ x10^{-2}$

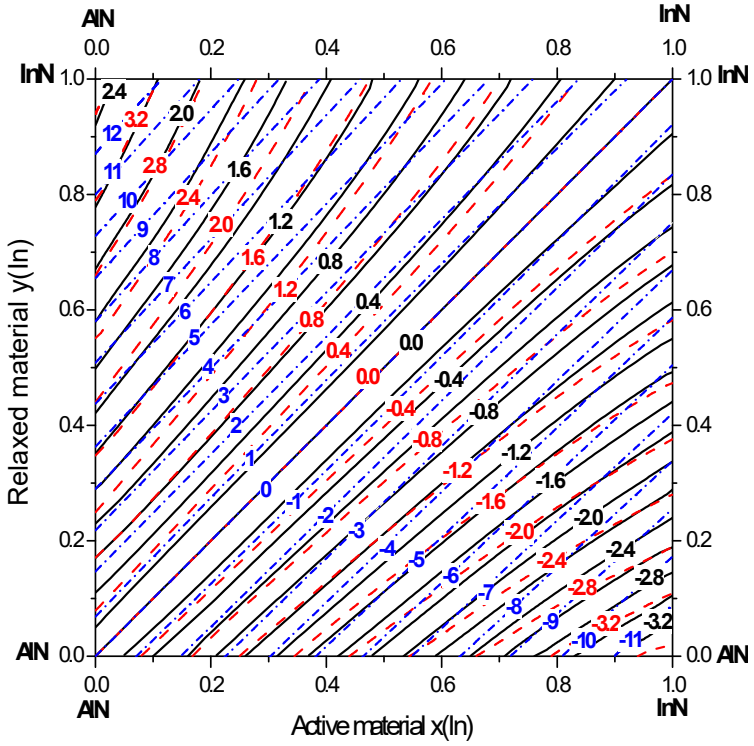

Figure 7: Strained (solid lines) and unstrained (dashed lines) conduction band offsets at $In_xAl_{1-x}N/In_yAl_{1-y}N$ heterointerfaces. In blue color are displayed the contour plots of lattice-mismatch induced strain (%).

3-2-4 Strained layers band gaps of $Al_xGa_{1-x}N$, $In_xGa_{1-x}N$ and $In_xAl_{1-x}N$

To further appraise this work and gain insight the behavior of the band offsets, it would be beneficial to carry out more information on the band structure parameters of the previously mentioned ternary nitride alloys. In fact, we have studied individually the variation of the band-gaps of $Al_xGa1_{-x}N$, $In_xGa_{1-x}N$ and $In_xAl_{1-x}N$ strained on $Al_yGa_{1-y}N$, $In_yGa_{1-y}N$ and $In_yAl_{1-y}N$ relaxed materials as a function of indium and aluminum compositions respectively.

Having properly determined the valence and conduction band offsets, energy band-gaps can be confidently analyzed using the relationship:

$$E_g^{str}(A_xB_{1-x}N) = E_g\left(A_yB_{1-y}N\right) + \Delta E_c(A_xB_{1-x}N/A_yB_{1-y}N) - \Delta E_v(A_xB_{1-x}N/A_yB_{1-y}N) \quad (18)$$

Results are depicted in figure 8. Here, we notify that the energy gap for a given ternary material of composition x, corresponds to the difference between the conduction and valence band positions $(E_c - E_v)$, i.e., for a fixed y composition, the energy of the gap is the length of the vertical line through x connecting the conduction and the valence bands.

As can be seen (figure 8(a)), when the binary GaN is used as relaxed material ($y = 0$), the band gap of the tensile strained-$Al_xGa_{1-x}N$ layer shows a red-shift in energy with increasing x relatively to its energetic position at zero strain. Indeed, the calculated energy

band gap of AlN strained on GaN is found to be about $5.7\ eV$ which is smaller than the $6.25\ eV$ well-known energy band gap value of relaxed AlN. In contrast, as one can observe from the same figure, using AlN instead of GaN as unstrained layer, the $Al_xGa_{1-x}N$ layer is subject to compressive strain and the corresponding band gap is slightly blue-shifted. The band gap energy value of GaN tensile strained on AlN becomes equal to about $3.63\ eV$.

Figure 8(b) plots the energy band gap of strained $In_xGa_{1-x}N$ on $In_yGa_{1-y}N$ versus x for y compositions ranging from 0 to 1. As can be deduced, the $In_xGa_{1-x}N$ band gap energy is considerably modified under tensile strain ($x < y$) and the GaN energy band gap value varies from $3.51\ eV$ ($x = 0, y = 0$) to $1.91\ eV$ for ($x = 0, y = 1$), i.e. the energy band gap of GaN is reduced when the material is tensile strained on InN. Furthermore, the calculated band gap of $In_yGa_{1-y}N$ slightly increases with increasing x when it is subject to compressive strain. Namely, for the strained-InN/relaxed-GaN interface, the InN band gap energy augments somewhat from $0.7\ eV$ at zero strain to about $0.74\ eV$ under strain.

In figure 8(c) is displayed the evolution of individual conduction and valence bands of $In_xAl_{1-x}N$ strained on $In_yAl_{1-y}N$. It is seen that when we consider the strained-$In_xAl_{1-x}N$ /relaxed-InN heterointerface, we found that the $In_xAl_{1-x}N$ band gap exhibits indeed a large deviation from its unstrained energetic position. One can deduce that the band gap of AlN tensile strained on InN is sharply reduced and becomes equal to about $3.28\ eV$. However, the band gap of InN compressively strained on AlN, is somewhat influenced by strain and takes the novel value of about $0.75\ eV$.

Table 3: $Al_xGa_{1-x}N$ ($In_xGa_{1-x}N$, $In_xAl_{1-x}N$) band gap bowing parameters and GaN (AlN, InN) strained band gaps. All values are in eV.

	unstrained	**Strained on GaN**	**Strained on AlN**	**Strained on InN**
$Al_xGa_{1-x}N$	$b = 0.62$ $E_g^{AlN} = 6.25; E_g^{GaN} = 3.51$	$b = 0.447$ $E_g^{AlN} = 5.71$	$b = 0.23$ $E_g^{GaN} = 3.63$	------ ------
$In_xGa_{1-x}N$	$b = 1.36$ $E_g^{GaN} = 3.51; E_g^{InN} = 0.7$	$b = 0.8$ $E_g^{InN} = 0.74$	------ ------	$b = 0.268$ $E_g^{GaN} = 1.91$
$In_xAl_{1-x}N$	$b = 2.5$ $E_g^{AlN} = 6.25; E_g^{InN} = 0.7$	------ ------	$b = 0.216$ $E_g^{InN} = 0.75$	$b = -0.946$ $E_g^{AlN} = 3.28$

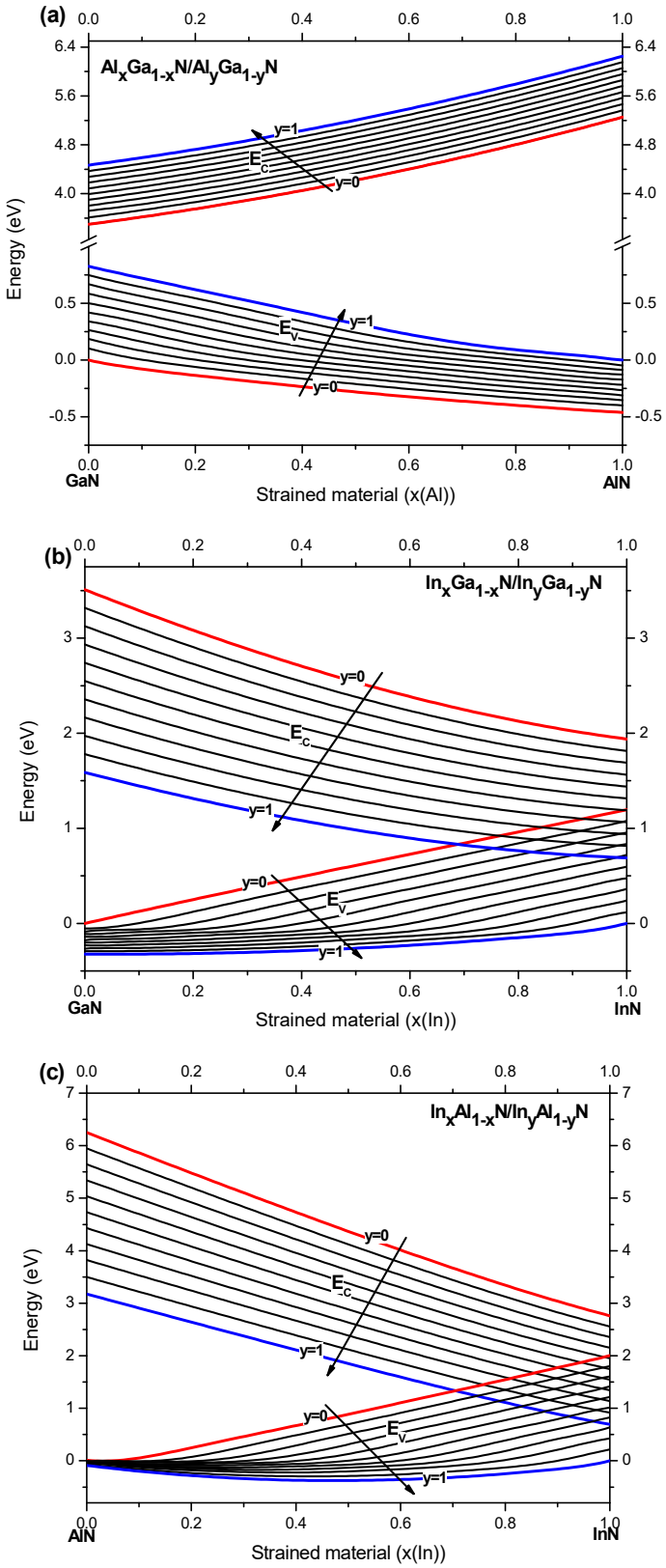

Figure 8: Calculated band gaps of: (a) $Al_xGa_{1-x}N$ strained on $Al_yGa_{1-y}N$, (b): $In_xGa_{1-x}N$ strained on $In_yGa_{1-y}N$ and (c) $In_xAl_{1-x}N$ strained $In_yAl_{1-y}N$. For a fixed x, the energy gap corresponds to the difference between the conduction and valence band positions of a selected y composition on the absolute energy scale of the figure.

4- DISCUSSION

Summaries of the calculated, unstrained and strained, valence and conduction band offsets of the binary interfaces AlN/GaN (GaN/AlN), InN/GaN (GaN/InN) and InN/AlN (AlN/InN) are listed in table 4. For selected interfaces, table 5 shows the valence and conduction band offsets calculated in this work along with the theoretical and experimental data available in the literature for comparison.

There are still large uncertainties in the reported band offsets of AlN/GaN (GaN/AlN) interfaces. The reported valence band offsets measured by different authors range from $0.15\ eV$ to $1.4\ eV$ **[37, 38]**. Photoemission measurements for VBOs at hexagonal structures yielded $0.6 \pm 0.24\ eV$ for GaN/AlN but it is not clear whether the interface is pseudomorphic **[38]**. Earlier measurements performed by the authors of reference **[39]** for a thin GaN film grown on hexagonal AlN yielded a VBO of $0.8 \pm 0.30\ eV$. Using the photoluminescence spectra, Baur *et al.* **[40]** obtained for the same interface a value of $0.5\ eV$. Recently, and using x-ray photoelectron spectroscopy, the authors of reference **[41]** determined a valence band offset value of $Al_{0.17}Ga_{0.83}N$/GaN to be $0.13 \pm 0.07\ eV$. The authors S. Schulz *et al.* **[42]** have combined experimental and theoretical studies to estimate, in the absence of strain, the values $-0.62\ eV$ and $2.19\ eV$ for AlN/GaN VBO and CBO respectively. Recently, the authors of reference **[43]** have directly determined the VBO of wurtzite C-plane and A-plane AlN/GaN heterojunction and they reported the values $-0.82 \pm 0.15\ eV$ and $0.63 \pm 0.15\ eV$ respectively. But anyway there are little experimental results of heteroepitaxy interface for no basal faces.

Concerning theory, from ab initio density functional methods, Satpathy *et al.* **[38]** calculated the VBO of $(GaN)_4/(AlN)_4$ heterostructure. They found a slight asymmetry between the band offset for the Ga-face and N-face interfaces with the VBOs being $1.15\ eV$ and 1.26 eV respectively. As reported in reference **[44]**, to determine the conduction band offset of $Al_xGa_{1-x}N$/GaN system, the authors assumed a linear interpolation for the unstrained valence band offset between $Al_xGa_{1-x}N$ and the binary GaN ($\Delta E_v = 0.8x\ [eV]$) and then estimated the following equation for the conduction band offset: $\Delta E_c = 0.603x + 0.99x^2\ eV$. In previous studies, K. Kishino and al **[45]** obtained a AlN/GaN conduction band offset value of $2\ eV$. Such a value was revised, using inter-band wavelength simulation, to be of $1.70 \pm 0.05\ eV$ **[46]**. As one can deduce from table 4, our calculated VBO and CBO results at the strained interfaces AlN/GaN (AlN/GaN) agree rather well with most of the experimental and reported values, mainly with references **[34]**, **[39]**, **[41]** and **[46]**. Moreover, we have obtained

a valence band offset at $Al_{0.17}Ga_{0.83}N/GaN$ of about $0.12\ eV$ and a conduction band offset value at AlN/GaN around $1.74\ eV$ which are in good accordance with the results reported in reference **[41]** and **[46]** respectively.

Table 4: Conduction and valence band offsets (eV) obtained in this work.

	AlN/GaN	**GaN/AlN**	**GaN/InN**	**InN/GaN**	**InN/AlN**	**AlN/InN**	**InN/GaN***	**AlN/GaN***	**InN/AlN***
ΔE_v^{uns}	-0.8	0.8	-1.05	1.05	1.85	-1.85	1.05	-0.8	1.85
ΔE_v^{str}	-0.46	0.824	-0.323	1.2	2.0	-0.09	1.2	0.96	2.0
ΔE_c^{uns}	2.0	-2.0	1.77	-1.77	-3.77	3.77	-1.77	2.0	-3.77
ΔE_c^{str}	1.74	-1.8	0.9	-1.57	-3.5	2.48	-1.76	0.88	-3.57

(*) values calculated applying the transitivity rule

Table 5: Conduction and valence band offsets (eV) of III-V wurtzite nitride interfaces.

	VBO			CBO		
	Exp	Theo	This Work	Exp	Theo	This Work
Strained GaN/AlN	0.60±0.24 [38] 0.8±0.3 [39] 0.50 [40]	1.15 ; 1.26 [38]	0.824			-1.8
Unstrained AlN/GaN	-0.62 [42]	-0.8 [44]	-0.8	2.19 [42]	1.593 [44]	2.0
Strained AlN/GaN	-0.82±0.15 [43]		-0.46		2.0 [45] 1.70±0.05 [46]	1.74
$Al_{0.17}Ga_{0.83}N/GaN$	0.13±0.07 [41]		0.12			
Strained InN/GaN	0.5-1.1 [47] 1.05±0.25 [48] 0.58±0.08 [13] 0.85 [49] 1.07 [50]	0.3-1.27 [47] 0.62 [35] 1.02 [48] 0.56 [51]	1.2	-2.22±0.10 [12] -1.68±0.10 [51]		-1.57
Unstrained InN/GaN		0.9[42]	1.05		-1.85 [43]	-1.77
InN/AlN	1.46 [54] 1.25 [55] 0.97 [56]	1.81±0.2 [48] 1.52±0.17 [52] 3.10±0.04 [53]	2.0		-4.0±0.2 [52]	-3.5

There is no consensus on the valence band offsets of InN/GaN, with the calculated values ranging from $0.3\ eV$ to $1.27\ eV$ and the experimental data from $0.5\ eV$ to $1.1\ eV$ **[47]**.

Earlier, Martin *et al.* **[48]** employed XPS to measure the valence band offset at InN/GaN heterojunction and obtained a value of $1.05 \pm 0.25\, eV$. In fact, they have included a correction term to cancel the piezoelectric effect. According to King *et al.* **[12]**, such a correction is based on a false assumption that the piezoelectric effects always act to decrease the magnitude of the valence band offsets. Recently, using high-resolution x-ray photoemission spectroscopy measurements, the latter authors **[12]**, have measured the valence and the conduction band offset of wurtzite InN/GaN heterojunction and obtained however, the value of $0.58 \pm 0.08\, eV$ and $2.22 \pm 0.10\, eV$ respectively and they propose a type I heterojunction between InN and GaN. Mahmood *et al*. **[49]** also, used photoemission measurements and found an InN/GaN valence band discontinuity of about $0.85\, eV$. Wang *et al.* **[50]** used capacitance-voltage and photocurrent spectroscopy and determined the valence and conduction band offsets to be 1.07 eV and $1.68 \pm 0.10\, eV$ correspondingly. Moses and Van de Walle reported a (0001) InN/GaN valence band value of $0.62\, eV$ **[35]**. Based on density functional theory (DFT) calculations using the generalized gradient approximation (GGA) and underestimated gaps, Shieh *et al.* **[47]** claimed that according to different strained conditions, piezoelectric polarizations can increase (compressive strain) or decrease (tensile strain) considerably the magnitude of the valence band offsets. They reported a (0001) VBO value equal to $1.02\, eV$ which is attributed to the case of strained-InN/Relaxed- GaN heterojunction. Similar calculations (DFT) to those performed by Shieh *et al.* but with the inclusion of gap adjusting external potential, Gorczyca *et al.* **[51]** extracted a VBO value equal to 0.56 eV for the 5/5 Superlattices. Recently and without taking into account strain and polarization fields, the authors of reference **[42]** reported the values $0.9\, eV$ and $1.85\, eV$ for the GaN/InN-VBO and -CBO respectively. We recall that we have calculated for the VBO and CBO at InN/GaN heterojunction the values around 1.2 eV and -1.57 eV respectively which are close to the average of the reported values.

Reasonable scatter exists between the scarce experimental and theoretical studies in determining the InN/AlN band offsets. Earlier experimental XPS studies developed by Martin *et al.* **[48]** propose a value of $1.81 \pm 0.20\, eV$. The authors of reference **[52]**, determined, using X-ray photoelectron spectroscopy, the wurtzite InN/AlN (0001) valence band offset to be $1.52 \pm 0.17\, eV$ to which they associated a conduction band offset of $-4.0 \pm 0.2\, eV$. The latter authors recommend a type I heterojunction between InN and AlN. However, from photoelectron spectroscopy (utilizing 110 eV incident photon), Wu et al. **[53]** found a significantly higher InN/AlN VBO of about $3.10 \pm 0.04\, eV$. Theoretically, Monch et al.

obtained a value of 1.46 eV determined from empirical tight bending calculations **[54].** VBO values of 1.25 eV and 0.97 eV are found separately using first-general potential linearized augmented plane wave method **[55]** and calculated from charge neutrality levels determined from green functions **[56]** respectively. For the same interface (InN/AlN), we obtained the values 2.0 eV for the valence band offset and 3.5 eV for the conduction band offset. They are comparable to the average of the reported values.

According to the authors of reference **[37,38],** the large spread between the different theoretical and experimental results could be the consequence of several factors such as uncontrolled strain effects or the difficulty of interpreting the photoemission spectra being the basis of the experimental results. We claimed that the discrepancies between our results and the published ones arise from the numerical parameter values used in our calculations and which most of them are available from theoretical calculations. Therefore we expect that more experimental data are necessary to confirm those theoretical parameters which still have some uncertainties.

Based on our obtained results, we can note a remarkable asymmetric VBO and CBO values obtained for the III-nitride symmetric heterointerfaces and we mainly attribute such behavior to strain and polarization-induced interface charges. Moreover, in table 4, we display values of the VBO and CBO of InN/GaN, AlN/GaN and InN/AlN calculated (i) directly using the model described beyond **[1]** and (ii) applying the transitivity rule **[27]**. As can be noted, the obtained results match only in some cases. It is clear that the transitivity rule is well fulfilled with unstrained interfaces and, yet, it may not be used to derive valence and conduction band offsets for strained systems. Indeed, band offsets actually depend on the in-plane lattice parameter. If the material members forming the interfaces would have the same lattice parameter or would be unstrained, the transitivity rule will be satisfied and consequently, band offsets are transitive in the case of unstrained and lattice matched systems (see table 4). However for heterojunctions having different lattice parameters, interfacial reactions occur and therefore, the transitivity rule may not necessary valid. As reported in reference **[52]**, the transitivity behavior is indeed expected for isovalent nitride systems, provided the heterojunctions are either fully relaxed or coherently strained on common in-plane lattice parameters. The authors of the same reference **[52]**, also claimed that the experimentally observed transitivity therefore suggests the presence of relaxed overlays, in agreement with our above contentions. The validity of our suggestion is also supported by a comparison of the $\Delta E_v(x)$ with published data for $In_xAl_{1-X}N$ alloys nearly lattice matched to GaN. We estimate, in the absence of strain, the VBO values $-0.46\,eV$ $(x = 0.17)$,

$-0.32\ eV$ $(x = 0.25)$ and $-0.23\ eV$ $(x = 0.3)$ which are in perfect agreement with results of references **[14, 42, 57]**.

Having discussed the VBOs and CBOs, we turn now and focus on the effect that strain and compositions have on the band gaps. As it is well known the most important parameter of semiconductor alloys is the band gap and its composition dependence. Our theoretical results indicate that in the case of alloys containing In ($In_xGa_{1-x}N$, $In_xAl_{1-x}N$), the bowing parameters is very affected by strain then in $Al_xGa_{1-x}N$. Moreover, one can deduce from table 3 that under tensile strain, the band gaps exhibit significant deviation and become particularly small compared to their unstrained values. Under compressive strain, our calculated band gaps of $In_xGa_{1-x}N$, $Al_xGa_{1-x}N$ and $In_xAl_{1-x}N$ are weakly enhanced compared with the situation without including strain. According to Gorczyca *et al.* **[53]**, the unusual decrease in the band gaps, notably with Indium contents, is found to stem from the In-induced changes in the states at the valence band top. Unlike the VBOs and CBOs at wurtzite binary nitride heterojunctions, there are practically no report on band offset data for wurtzite ternary nitride heterointerfaces. Our systematical calculations can provide useful information on the compositional dependence band offsets (equation (17) and table 2). They are also of great interest in designing lattice mismatched nitride based devices.

5- SUMMARY AND CONCLUSION

In conclusion, based on a theoretical model allowing the band structure calculation of strained quantum well wurtzite semiconductors and on the choice of a particular set of input parameters, we present estimation values of valence and conduction band offsets for lattice matched and pseudomorphically strained $Al_xGa_{1-x}N/Al_xGa_{1-x}N$, $In_xGa_{1-x}N/In_xGa_{1-x}N$ and $In_xA_{1-x}N/In_xA_{1-x}N$ heterojunctions. The effect of compressive and tensile strains on the band structure are studied and discussed. Where the tensile strain is applied, the magnitudes of the VBOs and CBOs, in the three studied heterojunctions, are strongly influenced suggesting a dominant effect of strain. However, with compressive strain the band offsets in the three studied cases, barely change. In fact, the tensile strain causes the VBOs to weaken, while compressive strain reinforces them. The defeat of the transitivity rule, often used to determine the band offsets in heterojunctions, was demonstrated and its cause was clarified. Overall, we have pointed out some interesting trends associated with nitrides and compared our results with previously published data. Although, more accurate and recent input parameters and further experimental and theoretical investigations are necessary to derive the correct band

offsets, our main band offset results provide valuable insight to band gap engineering and hence to processes of device optimization and design.

REFERENCES

[1] S. L. Chuang, and C. S. Chand, Semicond. Sci. Technol. **12**, 2525 (1997).

[2] S. Nakamura, M. Senoh, S.-I. Nagahama, N. Iwasa, T. Matsushita, and T. Mukai, Appl. Phys. Lett. **76**, 22 (2000).

[3] A. Bhouri, N. Yahyaoui, M. Debbichi, H. Mejri, J.-L. Lazzari, and M. Said, Phys. Status Solidi C **8**, No. 5, 1544 (2011).

[4] J. M. Barkera, D. K. Ferry, D. D. Koleske, and R. J. Shul, J. Appl. Phys. **97**, 063705 (2005).

[5] J. Wu, J. Appl. Phys. **106**, 011101 (2009).

[6] G. F. Brown, J. W. Ager III, W. Walukiewicz, and J. Wu, Sol. Energ. Mat. Sol. Cells **94**, 478 (2010).

[7] M. Tchernycheva, L. Nevou, L. Doyennette, F. Julien, E. Warde, F. Guillot, E. Monroy, E. Bellet-Amalric, T. Remmele, M. Albrecht, Phys. Rev. B **73**, 125347 (2006).

[8] E. Bellotti, K. Driscoll, T. D. Moustakas, and R. Paiella, J. Appl. Phys. **105**, 113103 (2009).

[9] M. Akazawa, T. Matsuyama, T. Hashizume, M. Hiroki, S. Yamahata, and N. Shigekawa, Appl. Phys. Lett. **96**, 132104 (2010).

[10] A. Bhouri, A. Rached, and J.-L. Lazzari, "Resonant tunneling transport in $Al_zGa_{1-x}N/In_xGa_{1-x}N/Al_zGa_{1-z}/In_yGa_{1-y}N$ quantum structures", to appear in Journal of Physics D: Applied Physics.

[11] W. Mönch, Electronic Properties of Semiconductor Interfaces, Springer, Berlin (2004).

[12] P. D. C. King, T. D. Veal, C. E. Kendrick, L. R. Bailey, S. M. Durbin, and C. F. McConville, Phys. Rev. B **78**, 033308 (2008).

[13] M. Akazawa, B. Gao, T. Hashizume, M. Hiroki, S. Yamahata, and N. Shigekawa, J. Appl. Phys. **109**, 013703 (2011).

[14] L. Cláudio de Carvalho, J. Furthmüller, and F. Bechstedt, Appl. Phys. Lett. **102**, 172105 (2013).

[15] W. Kohn, and L. J. Sham, Phys. Rev. **140**, A1133 (1965); J. P. Perdew, and Y. Wang, Phys. Rev. B **45**, 13244 (1992).

[16] J. P. Perdew, K. Burke, and M. Erzerhof, Phys. Rev. Lett. **77**, 3865 (1996); J. P. Perdew, K. Burke, and M. Erzerhof, Phys. Rev. Lett. **78**, 1396 (1997).

[17] S. Zhang, D. Tomnek, S. G. Louie, M. L. Cohen, and M. S. Hybertsen, Solid State Commun. **66**, 585 (1988); S. B. Zhang, M. L. Cohen, S. G. Louie, D. Tomanek, and M. S. Hybertsen, Phys. Rev. B **41**, 10058 (1990).

[18] D. Cociorva, W. G. Aulbur, and J. W. Wilkins, Solid State Commun. **124**, 63 (2002).

[19] C. Mietze, M. Landmann, E. Rauls, H. Machhadani, S. Sakr, M. Tchernycheva, F. H. Julien, W. G. Schmidt, K. Lischka, and D. J. As, Phys. Rev. B **83**, 195301 (2011).

[20] C. Mitra, B. Lange, C. Freysoldt, and J. Neugebauer, Phys. Rev. B **84**, 193304 (2011).

[21] A. Punya, and W. R. L. Lambrecht, Phys. Rev. B **88**, 075302 (2013).

[22] W. Chen, and A. Pasquarello, Phys. Rev. B **86**, 035134 (2012); Phys. Rev. B **88**, 119906 (E) (2013).

[23] C. G. Van de Walle, and R. Martin, Phys. Rev. B **34**, 5621 (1986); C.G. Van de Walle, Phys. Rev. B **39,** 1871 (1989).

[24] F. Ben Zid, A. Bhouri, H. Mejri, R. Tlili, and M. Said, J.-L. Lazzari, F. Arnaud d'Avitaya, and J. Derrien, J. Appl. Phys. **91** (11), 9170 (2002).

[25] A. Bhouri, F. Ben Zid, H. Mejri, A. Ben Fredj, N. Bouarissa, and M. Said, J. Phys.: Condens. Matter, **14**, 7017 (2002).

[26] A. Bhouri, H. Mejri, F. Ben Zid, H. Belmabrouk, M. Said, N. Bouarissa, and J.-L. Lazzari, J. Phys.: Condens. Matter. **16**, 511 (2004).

[27] A. Bhouri, A. Ben Fredj, J.-L. Lazzari, and M. Said, Superl. Microstr. **36**, 799 (2004).

[28] S. Ben Rejeb, A. Bhouri, M. Debbichi, J.-L. Lazzari, and M. Said, Superl. Microstr. **50**, 277 (2011).

[29] N. Binggeli, P. Ferrara, A. Baldereschi, Phys. Rev B **63**, 245306 (2001).

[30] K. Steiner, W. Chen, and A. Pasquarello, Phys. Rev B **89**, 205309 (2014).

[31] I. Vurgaftman, J. R. Meyer, and L. R. Ram-Mohan, J. Appl. Phys. **89** (11), 1 (2001); I. Vurgaftman, J.R. Meyer, J. Appl. Phys. **94**, 3675 (2003), and references therein.

[32] Q. Yan, P. Rinke, M. Scheffler, and C. G. Van de Walle, Appl. Phys. Lett., **95**, 121111 (2009).

[33] Anderson Janotti, and Chris G. Van de Walle, Phys. Rev. B **75**, 121201-R (2007).

[34] S. R. Lee, A. F. Wright, M. H. Crawford, G. A. Petersen, J. Han, and R. M. Biefeld, Appl. Phys. Lett. **74,** 3344 (1999).

[35] P. G. Moses, and C. G. Van de Walle, Appl. Phys. Lett. **96**, 021908 (2010).

[36] K. S. Kim, A. Saxler, P. Kung, M. Razeghi, and K. Y. Lim, Appl. Phys. Lett. **71,** 800 (1997).

[37] H. Li, X. Liu, J. Wang, D. Jin, H. Zhang, S. Yang, S. Liu, W. Mao, Y. Hao, Q. Zhu, and Z. Wang, J. Appl. Phys. **112**, 113712 (2012), and references therein.

[38] S. Satpthy, Z. S. Popovic, and W. C. Mitchel, J. Appl. Phys. **95** (10), 5597 (2004).

[39] G. Martin, S. strike, A. Bochkarev, A. Agarwal, A. Rockett, H. Morkoç, W. R. L. Lambrecht, and B. Segall, Appl. Phys. Lett. **65**, 610 (1994).

[40] J. Baur, K. Maier, M. Kunzer, U. Kaufmann, and J. Schneider, Appl. Phys. Lett. **65**, 2211 (1994).

[41] X. J. Wan, X. L. Wang, H. L. Xiao, C. M. Wang, C. Feng, Q. W. Deng , S.Q. Qu, J. W. Zhang, X. Hou, S. J. Cai, Z. H. Feng, Chin. Phys. Lett. **30** (5), 057101 (2013).

[42] Stefan Schulz, Miguel A. Caro, Lay-Theng Tan, Peter J. Parbrook, Robert W. Martin, and Eoin P. O'Reilly, Appl. Phys. Express 6, 121001 (2013).

[43] H. Li, X. Liu, L. Sang, J. Wang, D. Jin, H. Zhang, S. Yang, S. Liu, W. Mao, Y. Hao, Q. Zhu, and Z. Wang, Phys. Status Solidi B. **251** (4), 788 (2014).

[44] V. I. Litvinov, A. Manasson, and D. Pavlidis, Appl. Phys. Lett. **85** (4), 600 (2004).

[45] K. Kishino, A. Kikuchi, H. Kanazava, and T. Tachibana, Appl. Phys. Lett. **81**, 1234 (2002).

[46] L. Nevou, M. Tchernycheva, L. Doyennette, F.H. Julien, E. Warde, R. Colombelli, F. Guillot, S. Leconte, E. Monroy, T. Remmele, and M. Albrecht, Superl. Microstr. **40**, 412 (2006).

[47] C. C. Shieh, X. Y. Cui, B. Delley, and C. Stampl, J. Appl. Phys. **109**, 083721 (2011), and references therein.

[48] G. Martin, A. Botchkarev, A. Rockett, and H. Morkoc, Appl. Phys. Lett. **68**, 2541 (1996).

[49] Z. H. Mahmoud, A. P. Shah, A. Kadir, M. R. Gokhale, S. Ghosh, A. Bhattacharya, and B. M. Arora, Appl. Phys. Lett. **91**, 152108 (2007).

[50] K. A. Wang, C. Lian, N. Su, D. Jena, and J. Timler, Appl. Phys. Lett. **91**, 232117 (2007).

[51] I. Gorczyca, T. Suski, N. E. Christensen, and A. Svane, Cryst. Growth Des. **12**, 3521 (2012).

[52] P. D. C. King, T. D. Veal, P. H. Jefferson, and C. F. McConville, Appl. Phys. Lett. **90**, 132105 (2007).

[53] C.-L. Wu, C.-H. Shen, and S. Gwo, Appl. Phys. Lett. **88**, 032105 (2006).

[54] W. Mönch, J. Appl. Phys. **80**, 5076 (1996).

[55] S.-H. Wei, and A. Zunger, Appl. Phys. Lett. **69**, 2719 (1996).

[56] J. Roberston, and B. Falabretti, J. Appl. Phys. **59**, 3241 (2006).

[57] M. Akazawa, B. Gao, T. Hashizume, M. Hiroki, S. Yamahata, and N. Shigekawa, J. Appl. Phys. **109**, 013703 (2011).